Electron emission characteristics in p-H($1s$) collisions from numerical solutions of the time-dependent Schrödinger equation

Michal Chassid and Marko Horbatsch
Department of Physics and Astronomy, York University, 4700 Keele Street, Toronto, Ontario, Canada M3J 1P3
(Received 10 January 2002; published 25 July 2002)

The numerical integration of the three-dimensional time-dependent Schrödinger equation that appears in the impact-parameter approximation is carried out using a Fourier collocation method that is based on a splitting technique for the time evolution operator. The final wave function is analyzed in momentum space using a histogram approach. Singly and doubly differential cross sections for ionization as a function of polar emission angle and energy are calculated near the maximum in the total cross section, i.e., at 50–60-keV impact energy. They compare well with recent experimental results for intermediate and high electron emission energies, while some discrepancies remain at low energies due to the neglect of residual Coulomb interactions in the ionized wave packet. In order to achieve convergence and to reproduce experimental results at electron energies below 20 eV one needs to extend the calculations to final internuclear separations beyond 30 a.u.

DOI: 10.1103/PhysRevA.66.012714 PACS number(s): 34.10.+x

I. INTRODUCTION

The numerical solution of the time-dependent Schrödinger equation (TDSE) for ion-atom collisions has become an area of intense investigation in recent years. Various techniques have been applied and usually tested on the case of proton-hydrogen collisions. Traditional techniques include large-scale basis-set expansions, e.g., in the Sturmian basis [1], Gaussian basis [2], and multicentre atomic-orbital expansions [3,4]. A recently developed technique employs the automatic generation of optimized basis sets (basis generator method) [5], and has been used very successfully in systems that involve one electron, as well as many-electron problems within the independent-particle model at the level of time-dependent density-functional theory [6,7]. So far these techniques have been used almost exclusively to calculate total cross sections for excitation, charge transfer, and ionization. The situation is slightly different for antiproton-hydrogen collisions, where the problem can be analyzed using a single-center basis, and differential ionization cross sections were, e.g., calculated in a Sturmian basis approach [8]. A recent calculation for p-H($1s$) collisions makes use of a finite discretized Hilbert-space basis of target-centered continuum states in conjunction with target and projectile bound states [9]. This careful work allows one to appreciate the difficulties of extracting continuum information from two-center basis-set expansions.

In order to study differential ionization probabilities and cross sections for a two-center geometry it is advantageous to resort to a direct numerical integration technique. Earlier fully three-dimensional results were obtained using a coordinate-space finite-difference approach [10]. These calculations were motivated by interesting structures observed in measurements involving helium targets using the so-called cold target recoil ion momentum spectroscopy (COLTRIMS) technique [11]. The measurements of completely resolved longitudinal and transverse electron momenta for known heavy-particle kinematics put in question the validity of the traditionally employed classical trajectory Monte Carlo (CTMC) technique, certainly in the range of low energies where quasimolecular dynamics, charge transfer via tunneling, and ionization via orbital promotion become important. In fact, a comparison of CTMC calculations, as well as a perturbative quantum theory, namely, the continuum distorted-wave method (CDW) with experimental doubly differential cross sections for the p-H($1s$) collisions system shows that no *ab initio* theory has explained so far the details of electron emission below the matching velocity, i.e., for impact velocities of the order of classical electron orbit velocities or below [12]. Experimental data for longitudinal momentum distributions in 114-keV p-H collisions suggest that even at high impact velocities both models provide qualitative explanations, but that some discrepancies persist in highly differential ionization data [13].

Several groups are working at present on the numerical solution of the TDSE in a complete two-center geometry. In the work of Kolakowska and co-workers [14] total cross sections have been obtained both from a finite difference, as well as a Fourier collocation technique. Many excitation and state-selective charge-transfer cross sections have been calculated for p-H($1s$) scattering, and they compare reasonably well with basis-set calculations (which usually have some advantage when it comes to bound-state populations due to the exact incorporation of the bound states). These calculations obtain agreement for $n=1$, 2, 3 bound-state populations on projectile and target with other theories and with experiment at the 10% level. Significant differences exist for subshell populations, which indicates that these may be affected by the way the two-center continuum is treated. A substantial factor-of-two discrepancy between practically all theories and experiment remains unresolved for the production of Balmer-α radiation [15]. For the total ionization cross section there are discrepancies between the numerical calculations and other large-scale theories at the 10% level, and with experiment at the 25% level (a significant discrepancy, which indicates that either experiment underestimates the true ionization cross section or that a number of different solution techniques for the TDSE fail for various reasons and overestimate ionization). Thus, an important aim for these

calculations is to reach the 5–10 % accuracy level for total ionization, and to be completely flexible as far as ionization mechanisms are concerned. These calculations support the idea that the dominant contribution to ionization at small to intermediate impact parameters comes from the so-called potential saddle region [10,16], a finding that has considerable support from COLTRIMS experiments for singly charged ionic projectiles.

Important computational efforts in this respect have been made within partial-wave expanded two-center [17], and one-center methods [18]. The detailed comparison with CTMC calculations shows that if one goes beyond the microcanonical initial distributions in the ($\hbar=0$) semiclassical approximation, one can actually describe the ionization dynamics rather well at impact velocities above the matching condition [18,19]. Nevertheless, some limitations persist, such as the underestimation of backward scattering, as well as the fact that classical small-impact-parameter results at higher energies appear to involve more violent ion-electron interactions than what is observed in quantum calculations.

We mention in passing that there are other recent attempts to tackle the present problem without solving the TDSE explicitly. Apart from the mentioned CDW approximation (of which there are more versions than referred to in references [12,13]), there are attempts to tackle the problem in a Born approximation with improved final-state wave function [20], and a variational calculation in which a simple time-evolved wave function is projected onto a correlated final continuum state [21].

Our interest in the present work is to provide a detailed comparison with experiment at an impact velocity above matching where the total ionization cross section reaches its maximum. The emphasis is on differential electron emission cross sections, which will serve as a benchmark for the attempt to solve the TDSE numerically for the ionized electron wave packet. At the same time we wish to address the question of the discrepancy of elaborate theoretical total ionization cross sections with the most accurate measurements [22] at the 25% level that is significant, since all these theoretical data lie systematically above the experimental results (the CDW approximation represents a notable exception).

II. THEORY

The impact-parameter approximation allows one to reduce the three-body quantum collision problem to an explicitly time-dependent single-particle problem for the electron moving in the field of the nuclei following classical straight-line motion. The concern of this work is to propagate the solution of

$$i\hbar\frac{\partial}{\partial t}\psi(\mathbf{r},t)=-\frac{\hbar^2}{2m}\nabla^2\psi(\mathbf{r},t)+V(\mathbf{r},t)\psi(\mathbf{r},t), \qquad (1)$$

and to analyze the wave function at a sufficiently large internuclear separation after the collision. We employ atomic units in which $\hbar=e=m_e=1$. The electronic potential is defined using the straight-line trajectory $\mathbf{R}(t)=(0,b,z_0-v_Pt)$, where b denotes the impact parameter, v_P is the projectile velocity, z_0 is an initial separation chosen large enough to not affect the final results significantly, and

$$V(\mathbf{r},t)=-\frac{Z_T}{|\mathbf{r}|}-\frac{Z_P}{|\mathbf{r}-\mathbf{R}(t)|}. \qquad (2)$$

In the actual calculations we work in a center-of-charge frame as far as the longitudinal motion is concerned; i.e., both nuclei move with one half of the projectile velocity. The transformation from the target frame [in which (1,2) are written] to this frame is obtained by a boost of the wave function according to

$$\psi(\mathbf{r},t)\rightarrow\exp(iv_Pz/2)\psi(\mathbf{r},t), \qquad (3)$$

where we have ignored a position-independent energy phase. The potential energy becomes

$$V(\mathbf{r},t)=-\frac{Z_T}{|\mathbf{r}-\mathbf{R}_T(t)|}-\frac{Z_P}{|\mathbf{r}-\mathbf{R}_P(t)|}, \qquad (4)$$

where $\mathbf{R}_T(t)=(0,0,-z_0/2+v_Pt/2)$ and $\mathbf{R}_P(t)=(0,b,z_0/2-v_Pt/2)$.

The center of charge corresponds to the equiforce point in the symmetric collision system; for asymmetric systems one may wish to investigate which of the two reference frames is more convenient. The reference frame used presently is advantageous for small to intermediate impact parameters for which the majority of electrons winds up in the vicinity of the potential saddle region, unless the impact energy is increased beyond 100 keV. In this inertial frame the coordinate-space mesh is used optimally, and the propagation errors for the ionized electron distribution are reduced due to the appearance of smaller electron momenta.

One might think the method of solution should be Galilean invariant, in principle, in order to reflect a symmetry of the TDSE. Therefore, the question arises whether the numerical solutions carried out in different boosted frames are completely equivalent. Due to the limitations imposed in momentum space by the discrete Fourier-transform method Galilean invariance can be satisfied only for momenta included in the finite momentum mesh. The time propagation scheme described below is periodic both in coordinate and in momentum space. Periodicity in momentum space implies that components of the wave function accelerated beyond the available maximum momentum value will move rapidly in the opposite direction. This will lead to distortions of the wave packet. Therefore, the center-of-charge frame is deemed to be advantageous not only from the coordinate-space economy point of view, but also in order to reduce errors in momentum space. The price to pay for this reference frame is that the initial state, namely, a target H($1s$)-orbital has to be transported into the collision region, which can introduce errors of its own.

The Fourier collocation method [14,16,23] makes use of the fact that the time evolution operator can be approximated to second order in the time step Δt by a splitting according to

$$u(t+\Delta t,t)=\exp[-iH(t)\Delta t]\approx\exp(-iT\Delta t/2)\times\exp[-iV(t)\Delta t]\exp(-iT\Delta t/2), \quad (5)$$

where the Hamiltonian operator in Eq. (1) is expressed as $H=T+V$ with the momentum representation used for the kinetic energy $T=p^2/2$. An explicit time propagation can be achieved by switching back and forth between the coordinate and momentum representation: beginning a time step with the wave function ψ given in coordinate space one carries out a propagation with the free-particle kinetic energy over $\Delta t/2$ by going into p space where the kinetic energy becomes a multiplicative operator. Then one switches back to coordinate space for the propagation over Δt with the potential-energy part which is followed by another half-step with the kinetic energy in momentum space. This symmetrized form of the time evolution operator takes into account the noncommutativity of T and V up to order $O(\Delta t^2)$, and therefore permits norm conservation during the time propagation at the percent level when using time steps of the order of $\Delta t=0.05$ a.u. for the problem at hand.

To carry out this scheme one uses a Cartesian mesh in coordinate space combined with a conjugate mesh in momentum space, and the Fourier transforms can be achieved efficiently using so-called fast Fourier transform (FFT) algorithms. The Cartesian mesh forces one to deal with the Coulomb singularity in some way. In our implementation the Coulomb potential is not regulated explicitly, but a mesh is chosen in which the origin is avoided (in fact the $x=0$, $y=0$, and $z=0$ planes are excluded). Therefore, the Cartesian mesh is used as a regulator. A price to be paid for the computational efficiency is the loss of rotational symmetry in the target and projectile eigenstates.

Following the propagation of the entire wave function $|\psi(t)\rangle$ in the two-center geometry we are interested in projecting out the bound-state contributions so that we can analyze the ionized wave packet $|\phi(t_{\rm fin})\rangle$, i.e., the final wave packet that represents the ensemble of ionized electrons. We need to compute projections onto traveling atomic bound states, and to remove them from the wave packet. First, projections onto target and projectile eigenstates are computed according to

$$a^T_{nlm}(t)=\int \chi^*_{nlm}(\mathbf{r}-\mathbf{R}_T(t))\exp(-iv_P z/2)\psi(\mathbf{r},t)d^3r, \quad (6)$$

and

$$a^P_{nlm}(t)=\int \chi^*_{nlm}(\mathbf{r}-\mathbf{R}_P(t))\exp(iv_P z/2)\psi(\mathbf{r},t)d^3r, \quad (7)$$

where the integrals are approximated by a simple quadrature formula over the mesh. Then, a wave packet $\phi(\mathbf{r},t)$ is calculated to represent the ionized electrons by subtracting the bound-state components:

$$\phi(\mathbf{r},t)=\psi(\mathbf{r},t)-\sum_{n,l,m} a^T_{nlm}\chi_{nlm}(\mathbf{r}-\mathbf{R}_T(t))\exp(iv_P z/2)-\sum_{n,l,m} a^P_{nlm}\chi_{nlm}(\mathbf{r}-\mathbf{R}_P(t))\exp(-iv_P z/2). \quad (8)$$

For large times the wave packet $\phi(\mathbf{r},t)$ represents the ionized electrons in the center-of-charge frame and needs to be analyzed for its momentum and energy content.

An important issue concerns the eigenstates of the two one-center Hamiltonians that are used to extract and remove the bound projectile and target populations. Two options are available in this respect: (i) one can use the discretization of the exact atomic hydrogen H(nlm) eigenstates that are not eigenstates of the numerical Hamiltonian, or (ii) one can compute numerical eigenvectors of the discretized eigenvalue problem. The latter method is simple to implement for the H($1s$) ground state by an iterative procedure (propagation in negative imaginary time), but it is more involved for the excited states (one has to ensure orthogonality to the lower-lying numerical eigenvectors). We are less interested in the precise computation of bound-state probabilities and cross sections, and therefore use method (i). It should be noted that the computation of derivatives by the discrete Fourier method is nonlocal in coordinate space, and is very accurate in regions where the wave packet has a large magnitude, while in the tail regions it is less accurate than a traditional finite-difference method, as can be shown by one-dimensional examples (e.g., Gaussian wave packets). The lack of accuracy in the regions away from the center of the box is most likely caused by the periodic boundary conditions implied in the discrete Fourier method. The main advantage of this method is that it can be used even for relatively large spacings in coordinate space. When checking for the accuracy of the eigenvalue problem in coordinate space by this method one finds that the biggest errors occur along the Cartesian axes.

For a given mesh size that is achievable on present-day computers (such as, e.g., $N=256$ in each dimension) one has to determine an ideal coordinate spacing Δx. This optimum value depends on the one hand, on the demand to contain the ionized wave packet $\phi(\mathbf{r},t)$ inside a finite volume in coordinate space up to some acceptable final internuclear separation. On the other hand, there are considerations for the momentum mesh that follow from the choice of Δx at finite and fixed N that are discussed below. The accuracy of the Fourier collocation method depends on the following features: (i) the step size Δx in coordinate space, which also controls the maximum momentum that can be represented via $p_{\rm max}=\pi/\Delta x$; (ii) the dispersion relation for free nonrelativistic particles is satisfied well for momenta up to $p_{\rm max}$, but particles leaving at $p_{\rm max}$ wind up at $p_{\rm min}=-p_{\rm max}$, and vice versa; (iii) the step size in momentum space is controlled by Δx as well as the number of mesh points in a given dimension, i.e., $\Delta p=2\pi/N\Delta x$. As a consequence of these properties one should find for a given mesh size N the optimum range of values for Δx. We have found that the ionization probability as a function of Δx for a fixed number of mesh

points N is relatively flat in the case of small impact parameters, and varies for more distant collisions in such a way that a minimum can be observed. We have determined for $N=256$ that an optimum range of spacings occurs around $\Delta x \approx 0.25-0.3$. This corresponds to a momentum resolution of better than 0.1 a.u. COLTRIMS experiments usually observe well-resolved structures on this scale, and, thus, we conclude that the computational resolution is sufficient for the problem at hand.

For problems that involve ionization one has to worry about the limitations of a finite coordinate-space mesh. Indeed, for the mesh parameters given above one has a box of rather finite size that does not contain any high-lying Rydberg levels. When comparing the calculated projections onto $n=2$, 3, 4 principal quantum number shells we find that the computation of $n=4$ occupation probabilities is not reliable in the sense that the population of $n=4$ at projectile and target exceeds the expected $1/n^3$ scaling that is satisfied by the $n=2$, 3 populations. Therefore, we use as a cutoff for the sums in Eq. (8) the $n=3$ shell in order to avoid the introduction of artificial continuum structures, which would arise as a consequence of the subtraction of the $n=4$ shell with inaccurately calculated projections $\langle \chi^{P,T}_{n=4} | \psi(t) \rangle$. Our calculated state-selective capture and excitation cross sections are comparable with the published data of a similar calculation, which is based, however, on numerically accurate eigenstates [14] (our cross sections are systematically about 10% higher).

On the edge of the computational mesh in coordinate space we introduce an absorber. This is achieved by attenuating the wave function in each time-propagation step in a layer extending over six spacings Δx from every edge of the box. The attenuation is chosen to be gentle enough to avoid reflections and the associated buildup of standing waves. The absorption is not perfect, which can lead to some reentry of electron density at the other side of the mesh when the nuclei approach the mesh edge due to the periodic boundary conditions imposed by the FFT-based time propagation. The norm loss due to the arrival of fast ionized electrons can be monitored, and the overall conservation of the ionized electron charge can be confirmed by adding the losses to the norm of $|\phi(t)\rangle$.

In order to compensate for the use of the exact H(nlm) eigenstates, and the H($1s$) initial state, in particular, we need to apply a correction. Calculations were also carried out for a projectile charge of $Z_P=0$. The impact-parameter-dependent differential ionization probabilities were then corrected by subtracting this ''background'' result. This makes a substantial difference at large impact parameters only. The emission energy- or angle-dependent probabilities from the $Z_P=0$ calculations are essentially structureless. This correction procedure is important in order to obtain a realistic total cross section. Even though the computed corrected ionization probability shows an exponential decrease with impact parameter we find a somewhat large total cross section when comparing with other theories and experiments. Also we should note that our projections onto the exact hydrogenic eigenstates are subject to small-amplitude oscillations, i.e., when calculating bound-state populations accurately by this method one needs to apply a time-averaging process at least over time scales that correspond to the inverse of the energy difference between the $n=1$ and $n=2$ shells. For the ionized electron momentum distributions these fluctuations do not appear to play an important role.

The analysis of the final continuum electron wave packet $|\phi(t_{\rm fin})\rangle$ is carried out in momentum space. The momentum-space mesh allows us to measure differential probabilities with a finite resolution. While the computation of projections onto Coulomb waves is envisaged eventually in order to take into account at least one of the Coulomb centres, we have resorted to a histogram technique over the discrete momentum-space mesh. Each point on this mesh corresponds to a discrete free-particle momentum vector. The squared modulus of the ionized wave function $\langle \mathbf{p} | \phi(t_{\rm fin}) \rangle$ provides the probability to occupy this momentum vector. Therefore, histograms with a finite resolution can be calculated for differential probabilities in electron emission angle, emission energy or both, as long as the bin size is greater than the momentum mesh resolution permits.

We have also attempted a coordinate-space histogram technique in order to calculate the energy spectra without directional information about the emitted electron. These take into account the residual interaction of the ionized wave packet with the two-center Coulomb potential. It turns out, however, that the calculation of the kinetic-energy contribution by a Fourier technique in coordinate space leads to a broadening at low energies when compared to a momentum-space histogram. This leads us to the conclusion that the ionized wave packet—at least in the vicinity of the nuclei—is subject to quantum properties, i.e., it is governed by the uncertainty principle. Only in the limit of a density with very small curvature will quantum mechanics become unimportant for the ionized wave packet [16].

The measurement of the kinetic energy at a given location in space using the direct ($\mathcal{F}$) and inverse Fourier transforms ($\mathcal{I}$) in order to compute the local kinetic-energy density according to

$$\tau(\mathbf{r}) = \phi^*(\mathbf{r}) \mathcal{I}\left[\frac{p^2}{2} \mathcal{F}[\phi(\mathbf{r})] \right] \tag{9}$$

results in histograms with non-negligible negative kinetic-energy density contributions in regions close to the nuclei. To what extent these negative contributions are caused by inaccuracies in the construction of the ionized wave packet [subtraction of states that are not eigenstates of the discrete Fourier-method eigenvalue problem in Eq. (8)], or whether they represent a general difficulty with expression (9) is unclear at present. The definition of the kinetic-energy density is not unique, and one may have more success with the implementation of the positive definite operator that is obtained using Green's theorem, namely,

$$\tau(\mathbf{r}) = \tfrac{1}{2} |\nabla \phi(\mathbf{r})|^2. \tag{10}$$

This enables at least the calculation of energy-differential cross sections for slow electrons while taking into account the residual Coulomb interactions. We will report on such

calculations in a future work, but note that the calculation of expression (10) by FFT methods is problematic on our finite momentum mesh for large momentum values.

In order to monitor the importance of residual Coulomb interactions we have also calculated the time history of the kinetic- and potential-energy expectation values for both the complete wave packet $|\psi(t)\rangle$, as well as the continuum packet $|\phi(t)\rangle$. These quantities can be used in order to monitor the energy loss suffered by the projectile. While we have agreement with the previous findings of Grande and Schiwietz [24] for collision energies above 50 keV, we note that their one-center treatment is inappropriate at lower energies: the discretized continuum in this treatment may be appropriate to calculate the flux to the capture channels, but it is unable to account for the correct potential-energy contributions in the captured parts of the wave packet. The detailed analysis of energy loss is, however, beyond the scope of the present paper.

Obviously, the numerical propagation of the wave function is limited by the fact that the mesh is finite in coordinate space. One might argue that a pure momentum-space representation would be of a considerable advantage in this regard. Normally the momentum-space approach suffers from the fact that the potential energy becomes an integral operator and is too cumbersome to deal with efficiently. In this regard the two-center method of Sidky and Lin [17] offers a substantial advantage. Nevertheless, based on our experience with the Fourier method we remark that any numerical approach carries a heavy computational burden: in momentum space the problem of a wave packet spreading in coordinate space translates into an increased demand on the momentum resolution. The momentum-space wave function with its rather limited range of p values where it has significant magnitude carries the information about the propagation into extended spatial regions by acquiring structure at smaller and smaller Δp.

As a consequence, any general-purpose quantum propagation scheme will be limited when one desires to compute the expanding wave packet for internuclear separations at which the system becomes truly asymptotic. Our method, thus, is not able to compute accurately so-called cusp electrons that are believed to settle only at internuclear distances of thousands of a.u. (this conclusion is based on CTMC calculations). Another problem that we cannot settle easily is the reduction in transverse momentum that occurs for $v_P/2$ electrons over the same time scales. This problem should be amenable to the approximate propagation of the final wave packet by a Feynman propagator for a time-varying harmonic potential chosen to approximate the Coulomb saddle region.

One method to tackle the postcollision interaction problem is given by the semiclassical propagation of the ionized wave packet in the full two-center potential. In order to start this propagation one can determine locally on the coordinate-space mesh the average velocity for the given density $\rho(\mathbf{r},t_{\rm fin})=\phi^*(\mathbf{r},t_{\rm fin})\phi(\mathbf{r},t_{\rm fin})$ from the density ρ and the current density $\mathbf{j}$ via

$$\mathbf{v}(\mathbf{r})=\frac{\mathbf{j}(\mathbf{r})}{\rho(\mathbf{r})}. \tag{11}$$

We have calculated such velocity fields for the ionized wave packets at internuclear separations of 20–40 a.u. using a Fourier method analogous to Eq. (9). The results are encouraging only in the region of the maximum near the saddle velocity $v_P/2$. The results for the three Cartesian components of the local velocity field are reasonably independent of each other, and do generally represent the expected free-particle dispersion. For example, for the y component the results are consistent with zero velocity at the impact parameter $y=b$ at all times, and for other locations y_1 one finds the expected relationship between a particle created during the closest approach at $y=b$, and which has propagated freely to y_1 according to the local velocity found there at time t_1. Nevertheless, there are substantial deviations from this general trend at locations away from the saddle region, and particularly in the wider vicinity of the nuclei.

For the saddle region, however, we were able to carry out classical trajectory calculations in order to study the long-time evolution of those electrons. Our finding is that over thousands of atomic time units the $v_P/2$ electrons may not change their longitudinal momentum component significantly, but their transverse momenta are typically cut in half. This effect that is connected to the result that the average potential energy for the ionized wave packet is still considerable for internuclear separations of the order of 20–40 a.u. will also affect the electron energy distributions for soft electrons. For the saddle (or $v_P/2$) electrons the typical reduction is from 0.2 to 0.1 a.u. of transverse momentum, i.e., it does not have too much impact on the electron energy that is dominated by the longitudinal component.

III. RESULTS

In Fig. 1 we show the ionization probability as a function of impact parameter as calculated by the present procedure, i.e., by projecting out the exact traveling H(nlm) eigenstates for $n=1,2,3$ on target and projectile and calculating the norm of the remaining ionized wave packet. A cubic mesh with 256 nodal points was used in each direction, and a spacing of $\Delta x=\Delta y=\Delta z=0.25$ a.u. was used. The probabilities were corrected by subtracting an equivalent calculation for zero projectile charge, which resulted in an artificial ionized wave-packet norm of 0.002. The main contribution for this correction comes from the ground state that is represented inaccurately on the Cartesian mesh, and that also acquires the largest error in the calculation of projections due to the unresolved cusp structure at the nuclear positions. We include results for impact velocities of $v_P=1.5$ a.u., which correspond to an impact energy of $E_P=56.25$ keV (crosses connected by a solid line), as well as for $v_P=\sqrt{2}$ a.u., i.e., $E_P=50$ keV (diamonds).

It can be seen that the probabilities follow an exponential behavior at large impact parameters, and that they are in close agreement with the results of Toshima [2] for several large-scale two-center Gaussian basis-set representations. The comparison of the results for slightly different energies

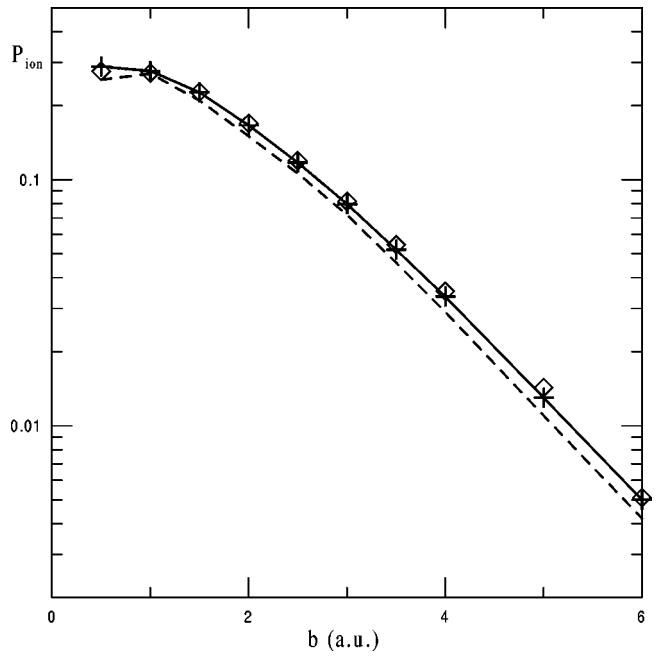

FIG. 1. Impact-parameter dependence of the ionization probability for p-H($1s$) collisions. Solid line with crosses, present calculation for 56 keV impact energy E_P; diamonds, present calculation for $E_P=50$ keV; dashed line, two-center Gaussian basis-set expansion results of Toshima [2] for $E_P=50$ keV.

(56.25 and 50 keV, respectively) shows that we are near the maximum of the cross section. Our total ionization cross section at 50 keV impact energy is calculated to be 1.97×10^{-16} cm^2, which is about 10% larger than the results reported by Toshima, namely, 1.78×10^{-16} cm^2. As explained below this discrepancy might be due to the fact that our ionized wave packet effectively includes Rydberg-state contributions, which, however, cannot be removed by simple projection. This is in contrast with the experimental data of Kerby *et al.* [12] at 48 keV (1.44×10^{-16} cm^2) who for this energy are in close agreement with the recommended values of Shah and co-workers [22] (1.4×10^{-16} cm^2). At higher energies Kerby *et al.* measured higher cross-section values than Shah and co-workers [22]. Therefore, they have a rather different energy dependence suggesting a peaking of the cross section at 70 keV. The experimental data of Shah and co-workers [22] have been compiled over many years (covering different energy ranges at closely spaced energy intervals), and have very good statistics. If indeed they are too low at (50–60)-keV impact energy, then a systematic error must be present which changes with the collision energy, since they connect smoothly to the high-energy Born limit. Incidentally the CDW ionization cross section is in agreement with the data given by Shah and co-workers for the total ionization cross section.

Other numerical calculations [14] also report cross sections that are higher than the experiments in the (50–60)-keV range. After a subtraction of the Rydberg contributions (which may be questionable) they arrive for 60 keV at total ionization cross sections of 1.87 and 1.73×10^{-16} cm^2 when using the finite-difference and Fourier methods, respectively. Fu *et al.* [9] obtain 1.58×10^{-16} cm^2 at 48 keV from their Hilbert-space discretization method. When we apply a complete Rydberg-series correction to our data based on our own $n=2,3$ cross sections and using $1/n^3$ scaling at 50 or 56 keV we arrive at an estimate for the ionization cross section of 1.68×10^{-16} cm^2 for both energies.

The consistency between the different theoretical ionization cross section results at the 10% level [around the value of 1.7×10^{-16} cm^2] coupled with a similar accuracy level for the bound-state cross section should serve as a guide for the accuracy that is achievable by the method. This finding is confirmed by the fact that the probabilities display a stability at this level against moderate variations in the mesh spacing. The latter finding does not preclude, however, that there could be a systematic error in the results. Our meshes are larger than the Fourier mesh employed in Ref. [14] (which uses a spacing of $\Delta x=0.385$ a.u., and 135 points in each dimension). However, when comparing our bound-state cross sections for $n=1,2,3$ on projectile and $n=1,2$ on the target we find that our results are typically 10% above those of Kolakowska *et al.* [14], particularly for target excitation. We assume that the overestimation of the target excitation cross sections is a price to be paid in our method for propagating an initial H($1s$) state that has not been tuned to satisfy the mesh Hamiltonian eigenvalue problem.

It is not straightforward to assess the accuracy of the ionization probability itself in our method. The biggest uncertainty arises from the need to choose a border between bound states and continuum, i.e., the decision to draw the line at the $n=3$ level in the subtraction of bound states in Eq. (8). Kolakowska *et al.* [14] have attempted an estimate for $n>3$ contributions at target and projectile, which is based on CTMC results that scale as $1/n^3$. Our own estimate of these contributions based on the $n=3$ probabilities, show that the CTMC-based estimates could be too low by a factor of 2 for the target. Our differential cross sections have to be considered carefully from the point of view that no subtraction has been made for the $n\geqslant4$ shells in $|\phi(t_{\rm fin})\rangle$. Comparison with experiment has to serve as a guide in order to establish the validity of this procedure. We use a logarithmic scale for the cross-section plots so that the normalization problem can be corrected visually.

In Fig. 2 the time evolution of the kinetic- and potential-energy expectation values for the ionized wave packet is shown for times after the closest approach for the case of $b=1$ a.u. and $v_P=1.5$ a.u. The data are taken from a calculation on a mesh of size $256\times256\times128$ and coordinate spacings of $\Delta z=\Delta y=0.35$ a.u. in the longitudinal z direction and the transverse direction y in the impact-parameter vector plane, and $\Delta x=0.5$ a.u. in the plane perpendicular to the scattering plane. The data are shown to illustrate several points: (i) the conversion of kinetic into potential energy for the ionized electrons is far from over even at internuclear separations beyond 40 a.u.; (ii) for the second half of the graph, i.e., at internuclear separations beyond 25 a.u. the calculated expectation value for the kinetic energy (and therefore also for the total energy) begins to suffer from the absorption of the fastest electrons at the mesh edges; (iii) the potential-energy expectation value for the ionized wave

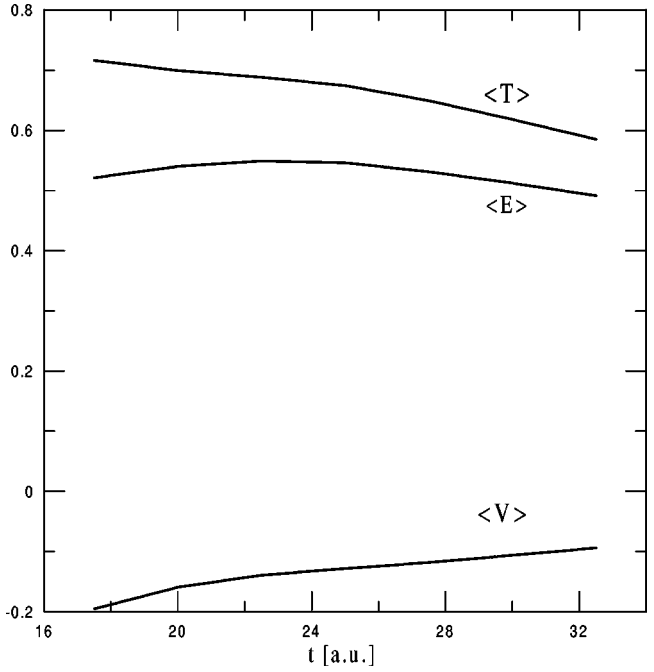

FIG. 2. Time evolution of the kinetic- ($\langle T \rangle$), total- ($\langle E \rangle$), and potential-energy ($\langle V \rangle$) expectation values given in atomic units for the ionized wave packet in $b=1$ a.u. p-H($1s$) collisions at $v_P=1.5$ a.u.

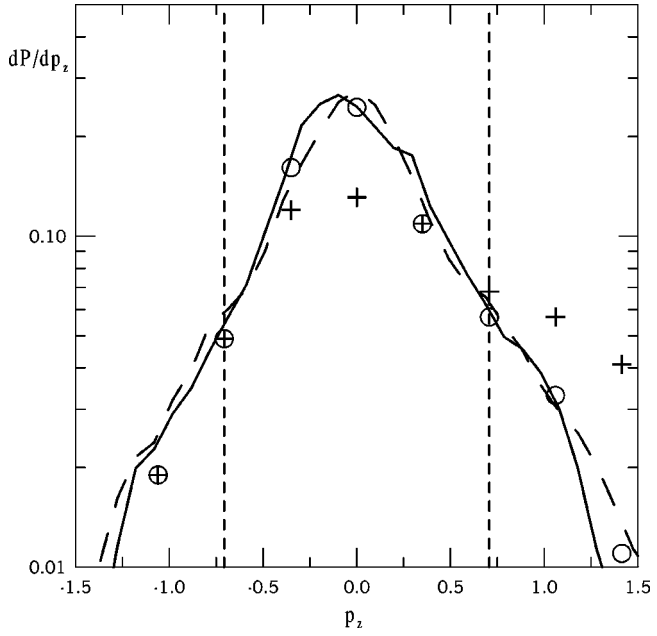

FIG. 3. Longitudinal momentum distribution for $b=1.2$ a.u. p-H($1s$) collisions at $v_P=1.414$ a.u. for two different final internuclear separations. Dashed curve, $R\approx 16$ a.u.; solid curve, $R\approx 30$ a.u. Crosses, TCMSD results; circles, CTMC results both from Fig. 1 in Ref. [19] for $b=1.2$ a.u. at 50-keV impact energy and final separation of $R=30$ a.u. The differential probabilities are given in atomic units. The target and projectile velocities are marked by short-dashed vertical lines.

packet is proportional to the inverse time after the closest approach (or to the inverse internuclear separation), as the slow electrons continue to experience primarily the target potential. At the largest internuclear separation shown the residual average potential energy in the ionized wave packet is close to 2.5 eV.

We note that the average total energy would remain constant after $t=22$ a.u., if it were not for the absorption of the fastest electrons at the mesh edges. This implies that one has to do the analysis of ejected electrons at least at two times: at around $t=22$ a.u. one should record the probability content for fast electrons, while the slow electrons need to be analyzed at a later time when they have propagated away from the nuclei, and thereby reduced their potential energy.

Given that we calculate the differential electron emission information from histograms in momentum space, i.e., using a free-particle basis, we stress the following limitations of our method: (i) we are not able to make accurate predictions about very soft electrons, as we cannot go to sufficiently large separations; (ii) the same statement holds for so-called cusp electrons, i.e., unbound electrons that follow very closely the projectile proton; (iii) to obtain accurate electron energy spectra we need to combine the information about fast electrons extracted at shorter final separations with the information about slow electrons extracted at larger separations when the error made by neglecting the residual potential energy is smaller.

We have also calculated the deviation from the average kinetic energy, and have found that for all impact parameters it is of the same order as the average itself. This follows as a result of distributions with maxima at (or near) zero energy and with substantial tails at high electron energies. This information can be used to compute the energy loss and straggling due to ionization in ion-atom collisions [24].

In Fig. 3 we show the time evolution of the longitudinal momentum distribution in our calculation for $v_P=1.414$ a.u. i.e., at 50 keV for an impact parameter of $b=1.2$ a.u. This parameter choice allows us to compare directly with other published results. Our data are shown for the internuclear separations of $R_z\approx 16$ and $R_z\approx 30$ a.u., which correspond to the times of 17.5 and 27.5 a.u. respectively, i.e., to the onset of the plateau in the average energy of the ionized wave packet (dashed line), and the end of the graph shown in Fig. 2, when the average residual binding energy has fallen below 3 eV (solid line). The momentum distribution is shown in the center-of-charge frame in which the calculation is performed, i.e., $v_e=v_P/2$ corresponds to $p_z=0$ in the graph, the target velocity is given by $p_z=-0.707$ a.u., while the projectile velocity is found at $p_z=0.707$ a.u.

We notice the strong presence of $v_P/2$ electrons at the earlier time with the tail of the distributions extending beyond the target and projectile velocities. As the system separates the longitudinal momentum distribution changes in such a way as to bring the electron momenta closer to the target proton. It is the result of an asymmetric distribution of the ionized electrons in coordinate space after closest approach. This occurs at the impact velocity of $v_P\approx 1.4$ a.u., which is above the matching velocity. The ionized electrons are physically closer to the target nucleus, and therefore the initially symmetric distribution over longitudinal momenta

experiences a deformation even late during the collision. This feature makes the analysis of final electron momentum distributions in momentum space somewhat difficult, and one has to be careful with the assessment that at a separation of $R=20$ a.u. matters are settled in p-H collisions [10,17]. For lower impact velocities (and small to moderate impact parameters) this effect is less pronounced, as the so-called saddle electrons are not only produced around $v_P/2$, but are geometrically truly in the vicinity of the potential saddle. Therefore, they suffer much less from postcollision interaction in the longitudinal direction than what is observed in the present case.

An important observation concerns the immediate ranges of the target and projectile velocities, i.e., $p_z \approx v_T$ and $p_z \approx v_P$. The distributions that are summed over both transverse directions, i.e., over y and x do not show any particular structures, i.e., cusps, for matching velocities. One can notice for the later time a slight drop in the probability for the faster electrons. Assuming the $v_e = \pm 1.25$ a.u. electrons were produced during closest approach at the origin they would have traveled distances of about $z = \pm 28$ a.u., respectively. Our mesh absorbs at distances of the order of $\pm 128 - 6 \times 0.25$, i.e., at 30 a.u. for the present calculation. Thus the drop of probability in the solid line as compared to the dashed line at large longitudinal momenta is clearly a consequence of the absorbing boundary condition at the mesh edge.

When comparing our results to recent work in the so-called two-center momentum-space discretization method (TCMSD) of Sidky and Lin [17,19] we find significant discrepancies both in the saddle region and at electron velocities faster than the projectile. The TCMSD results predict a rather substantial fraction of electrons faster than the projectile. The CTMC results from Ref. [19], on the other hand, appear to be rather close to our result at the shorter internuclear separation (even though they were obtained at a separation that corresponds to our $R \approx 30$ a.u. result).

One may wish to speculate about the origin of the difference in results between the present calculation and the TCMSD approximation. There might be problems with breaking up the wave function into two contributions centered on each nucleus. The Gaussian basis calculations of Toshima [2] (and previous two-center atomic-orbital calculations as well) have demonstrated a nonuniqueness in terms of how much ionization flux is supported by either center as a function of the basis size. While this is not necessarily critical when it comes to total-cross-section calculations, it is very critical for the calculation of the electron emission characteristics (a topic discussed in Ref. [9]). One would have hoped that the flexibility of the TCMSD method would allow the calculation to determine the correct amount of ionized electrons associated with projectile and target. The comparison with our result (which is not biased in this respect) indicates that this might not be the case. The ultimate test for the method (and for our calculations as well) will come from comparison with experiment in Fig. 3, i.e., when experiments such as reported in Ref. [13] are carried out at lower collision energies. It will also be important to compare results from the present approach to all the data calculated by Sidky and Lin in order to arrive at more general conclusions.

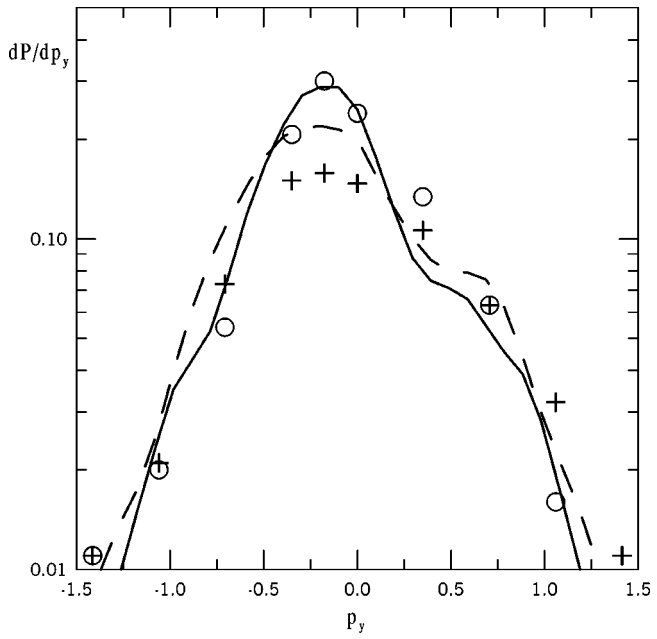

FIG. 4. Transverse momentum distribution in the scattering plane defined by the impact-parameter vector for $b=1.2$ a.u. p-H($1s$) collisions at $v_P=1.414$ a.u. for two different final internuclear separations. Dashed curve: $R \approx 16$ a.u.; solid curve: $R \approx 30$ a.u. Crosses, two-center momentum-space discretization method results; circle, CTMC results both from Fig. 1 in Ref. [19] for $b=1.2$ a.u. at 50-keV impact energy and final separation of $R=30$ a.u. The differential probabilities are given in atomic units.

Figure 4 shows the corresponding two snapshots of the transverse momentum distribution in the y-z scattering plane which is defined by the impact-parameter vector. These distributions again agree better with the classical results presented in Ref. [19] than with the quantum TCMSD calculations. At the relatively high impact velocity considered in the present work the time evolution of this distribution is not as dramatic as it may be in the quasimolecular regime where interference between dominant ionization paths may lead to a beating pattern between electrons emitted in the direction of the projectile, and in the opposite direction [25]. We notice an asymmetry in the distributions: there is a main peak at momenta that correspond to electron motion in the opposite direction to the projectile deflection from the nucleus; in addition one observes a shoulder that corresponds to electrons following the direction of the scattered projectile. Both these features are also present in the classical and quantum calculations of Ref. [19]. The TCMSD calculation has a smaller total ionization probability as compared to the CTMC and to the present results.

The ionized electron wave packet is produced predominantly in the center-of-charge frame with substantial transverse components. As the nuclei separate the distribution of free-particle momenta narrows in the transverse direction. The time evolution of the distributions is controlled by two effects: (i) the true meaning of the projection method (4) is valid only for separations when the predominantly occupied inner orbitals acquire an insignificant overlap with the ionized wave packet; (ii) the ionized electrons with definite en-

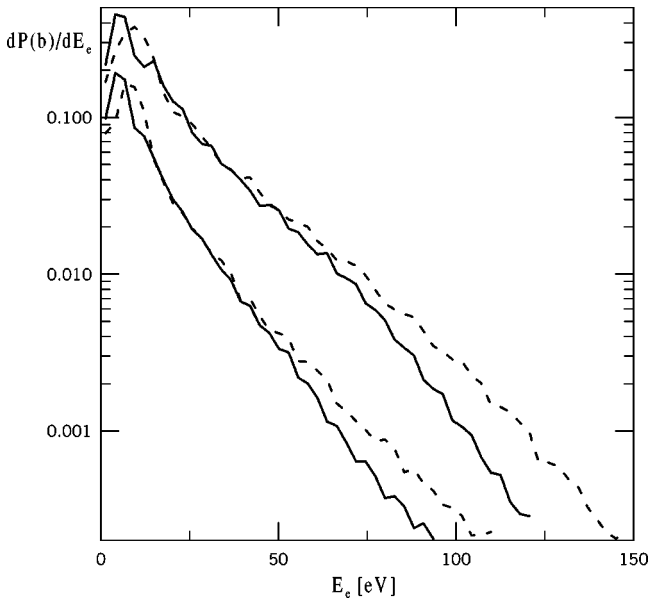

FIG. 5. Impact-parameter-dependent differential electron emission probabilities (in atomic units) as a function of electron energy in eV for 56-keV p-H collisions and two impact parameters; top pair of curves, $b=1$ a.u.; bottom pair, $b=3$ a.u.. The dashed curves are for an internuclear separation of 16 a.u., while the solid curves are for 31 a.u.

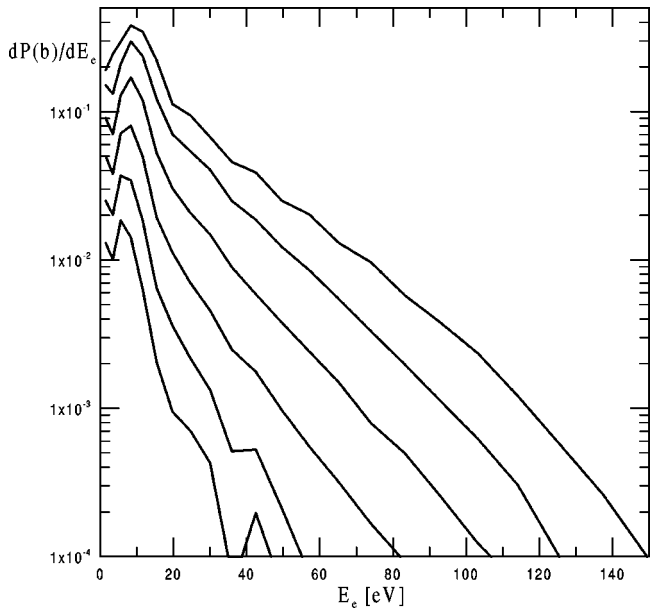

FIG. 6. Impact-parameter-dependent differential electron emission probabilities (in atomic units) as a function of electron energy in eV for 56-keV p-H collisions. From top to bottom results for $b=1,2,3,4,5,6$ a.u. The probabilities are given in a.u., and are calculated at an internuclear separation of 16 a.u.

ergy must have higher kinetic energies during the collision than asymptotically, since they give up some kinetic energy while they leave the two-center Coulomb potential; (iii) post-collision interaction effects can be responsible for a shift in the longitudinal peak position. These effects are not easily untangled. In fact, we find that the more distant collisions lead to longitudinal distributions which shift closer to the target position as the projectile proton moves away. The use of the center-of-charge frame in the longitudinal direction may actually be a slight disadvantage in this case as compared to the target frame. At large momenta $|p_y|>1.25$ a.u. we notice again the drop in probability at the later time due to the absorbing mesh boundary.

In order to illustrate the effect of the final internuclear separation on the analysis problem we show in Fig. 5 our results for the singly differential energy-dependent probability for two impact parameters, namely, $b=1$ and $b=3$ a.u. at two times (or nuclear separations) that correspond approximately to those used in Figs. 3 and 4 (for 50 keV). It can be seen that the shift in the peak location in the longitudinal momentum distribution from the $v_P/2$ position towards the target proton momentum results in a shift of the maximum in the differential probability towards lower electron energies. Thus, the low-energy electron energy distribution cannot be calculated reliably at small final separations without taking the Coulomb interaction into account. On the other hand, one can notice a deterioration of the distribution for larger electron energies with increasing internuclear separation: the absorption of electron density at the boundaries (particularly in the direction perpendicular to the scattering plane due to the reduced mesh size in this dimension) results in a removal of fast electrons from the analyzed ensemble. Therefore, the distributions should be corrected by splicing together the probabilities for fast electrons (e.g., for energies above 30 eV in the target reference frame) for an internuclear separation of the order of 16 a.u., while the low-energy electron continuum is to be calculated at larger internuclear separations, such as 31 a.u.

In Fig. 6 we show a selection of impact-parameter-dependent ionization probabilities as a function of electron energy after the subtraction of the background calculated from an equivalent time propagation without projectile potential. We note that smaller values of $b=1$, 2 which are the dominant impact parameters for the ionization cross section are characterized by a maximum associated with the saddle mechanism ($v_P/2$ electrons have on average 7.7-eV kinetic energy in the target reference frame assuming a small amount of transverse momentum). For larger impact parameters the peak moves towards lower energies. Note that these peaks move to lower energies when the system is propagated to larger distances (cf. Fig. 5). The graph also demonstrates clearly how the smaller impact parameters are responsible for all fast electrons. Once one moves to an impact parameter of $b=6$ a.u., it becomes very unlikely to produce electrons with energies larger than 30 eV.

In Fig. 7 we present results from an integration over impact parameter using

$$\sigma(E)=2\pi\int_0^\infty bdbP_E(b). \tag{12}$$

A total of 10 b values was used to approximate the integral in Eq. (8) by a finite sum with an interval of $\Delta b=0.5$ a.u. in the range where the weighted probability has large contributions. This b mesh was found to provide sufficiently accurate re-

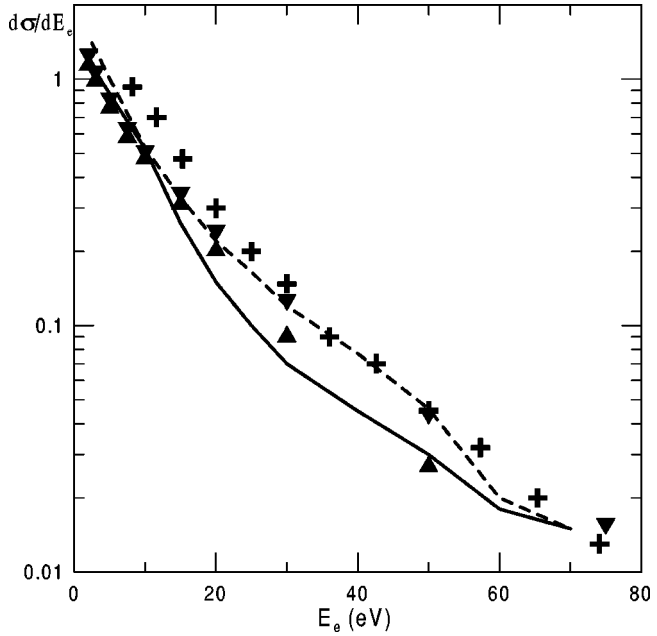

FIG. 7. Singly differential cross section for electron emission as a function of electron energy. Solid triangles and inverted triangles: experimental results of Ref. [12] for 48- and 67-keV impact energy, respectively. Crosses: present results for 56 keV. The cross sections are given in 10^{-17} cm^2/eV. Solid line and dashed line: Discretized finite Hilbert-space basis calculation and Born approximation, respectively, taken from Ref. [9].

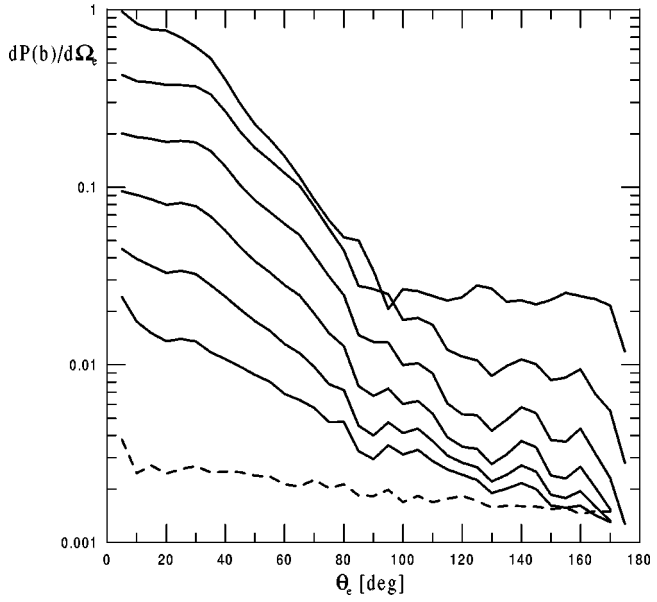

FIG. 8. Impact-parameter-dependent differential electron emission probabilities as a function of polar emission angle in degrees for 56 keV p-H collisions. Solid lines from top to bottom results for $b=1,2,3,4,5,6$ a.u. Dashed line: reference calculation for $Z_P=0$, which is used to subtract the background.

sults given that the differential probabilities shown in Fig. 6 are relatively smooth. We do not include results below 8 eV, as the structures at lower energies are considered an artifact of the present method, which extracts information from the propagated wave function using a free-particle basis at finite internuclear separation.

The comparison with the experimental data for 48- and 67-keV impact energy shows that our calculated results are very consistent with them in shape at least for electron energies above 8 eV. Good agreement was found by CDW calculations [26], and with CTMC calculations that were patched with first-order Born approximation results [12]. The present data overestimate the experimental data by about 40%, which is consistent with the total-cross-section ratio. The shape of the cross section fits nicely in between the 48 and 67-keV data, and in this sense agrees slightly better with them than the calculation of Ref. [9] in which the continuum parts of Hilbert space are discretized in a target-centered complex exponential basis. One can argue that an average energy of about 2.5 eV is folded into our calculation due to the residual potential energy as indicated for one impact parameter in Fig. 2. A naive correction of our calculated results at low energies would involve a shift of the theoretical curve to the left by 2.5 eV.

In Fig. 8 we present our impact-parameter-dependent probabilities that are differential in the polar emission angle. One can notice from the histogram that the Cartesian uniform mesh is not ideal for this type of measurement, and that one has to be careful in not overinterpreting apparent structures at 90° or 180°. Substantial backscattering contributions come from impact parameters below $b=2$ a.u. The results for larger impact parameters are not as dramatically different as one might have expected (the sideways tug that the electron density experiences might have led one to believe that larger emission angles would be strongly preferred in distant collisions). Actually, when one calculates the electron emission probabilities in the center-of-charge frame, they turn out to be rather flat, i.e., independent of the polar emission angle in this frame. The forward-backward asymmetry is mostly an effect of transforming the results to the target frame. This observation supports the notion that the ionized momentum distribution is generated first in this frame (as it is easiest to have an unbound particle in this frame while the nuclei are still close by, an idea explored in Ref. [19]). As the nuclei separate the ionized electrons in the more distant collisions interact predominantly with the target nucleus and are pulled back to yield what looks like target ionization by a perturbation.

In Fig. 9 we display the singly differential cross section as computed from the probabilities shown in Fig. 8, and compare them with the experimental results for $E_P=48$ and 67 keV. One can notice the overall good agreement: electrons are ejected predominantly in the forward direction, and a plateau can be observed for backward scattering. For scattering in a small window at 180° our calculations predict a drop in the cross section, which is not observed in the perturbative Born or CDW theories. We have found this behavior to be consistent as the initial and final internuclear separations were increased. This behavior needs to be explored further by calculations with a better resolution in momentum space.

In Fig. 10(a) we present the most sensitive quantity available in p-H$(1s)$ ionization experiments so far [12], namely, the doubly differential electron emission cross section as a

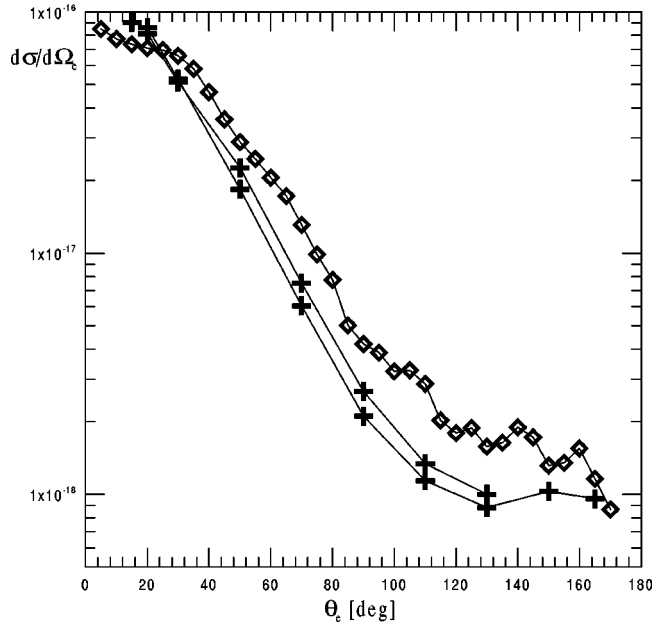

FIG. 9. Singly differential cross section for electron emission as a function of polar emission angle. Crosses: experimental results of Ref. [12] for 48 keV (bottom) and 67 keV (top) impact energy, respectively. Diamonds: present results for 56 keV. The cross sections are given in cm^2/sr and were calculated at a final separation of 16 a.u.

function of electron energy for five different emission directions. The theoretical results are for a slightly higher energy, and thus they have somewhat stronger high-energy electron contributions, most notably at forward angles. Theory and experiment coincide in the most important trends: a nearly exponential falloff of the cross sections with electron energy can be observed with larger decay constants as one goes from forward to sideways emission. At medium to high electron energies we observe a good consistency in the spacings between the respective results. However, some systematic deviations can be observed at low energies: for forward emission the theoretical results for 10° and 30° predict a merging of the cross sections below 40 eV; the experimental results for 15° and 30° are very close between 30 and 40 eV but deviate by a factor of 2 between 10 and 20-eV electron energy. For emission perpendicular to the beam axis we also find some discrepancy at energies below 20 eV. At higher energies our curve agrees well with experiment apart from fluctuations that are deemed to be insignificant, and which show limitations of the histogram approach. Between 10 and 20 eV our results are a factor of 2 higher than experiment.

The present comparison of theoretical data with experiment on the doubly differential cross section is similar to the comparison between CDW and CTMC/Born results given in Fig. 4 of Ref. [12]. The CDW results given in Ref. [12] for 48-keV impact energy follow the trend of the experimental data for 50° at all energies, but underestimate the cross section in the forward direction for energies below 20 eV. In fact, it appears as if the failure of the CDW cross section to rise at low energies in the forward direction is the consequence of strong projectile electron contributions. A careful

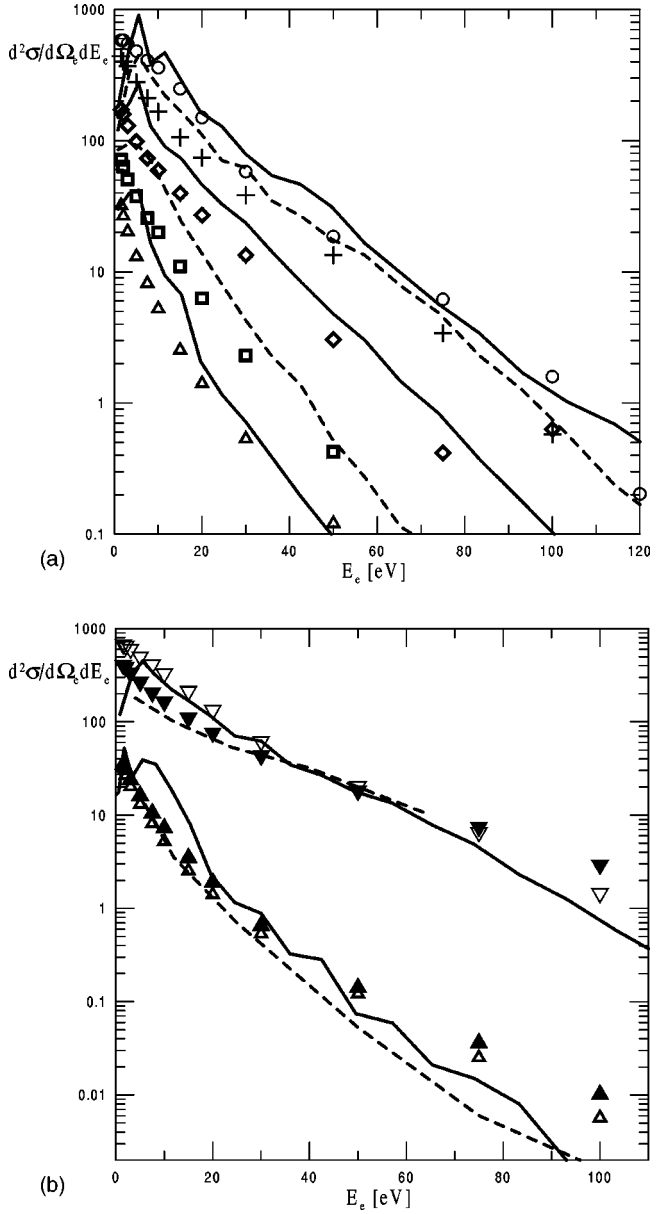

FIG. 10. (a) Doubly differential cross section for electron emission in 56-keV *p*-H collisions (theory) as compared to the experimental 48-keV results (in units of 10^{-20} cm^2/sr/eV). Solid lines from top to bottom: present calculation for the polar emission angles of $\theta_e = 10°, 50°, 90°$; dashed lines: corresponding results for 30° and 50°. Experimental data from Ref. [12]: circles, 15°; crosses, 30°; diamonds, 50°; squares, 70°; triangles, 90°. (b) Doubly differential cross section for electron emission in 56-keV *p*-H collisions (theory solid line) at two emission angles (30° and 90°) in comparison with experiment at 48 and 67 keV [12] and with the CDW approximation from Ref. [12] (dashed line) at 48 keV (in units of 10^{-20} cm^2/sr/eV). Inverted open triangles, experiment at 48 keV and $\theta_e = 30°$; inverted solid triangles, experiment at 67 keV and $\theta_e = 30°$; open triangles, experiment at 48 keV and $\theta_e = 90°$; solid triangles, experiment at 67 keV and $\theta_e = 90°$.

examination of the doubly differential cross section (which would require additional experimental investigations at emission angles of 10° and less) will therefore provide strong clues about systematic difficulties of the CDW method in

this energy range.

In Fig. 10(b) we illustrate the comparison by showing results two angles at both 48 keV and 67 keV. The CDW results from [12] are shown for 48 keV and illustrate the points made above: for sideways emission (90°) both the CDW and the present cross sections have a shape that is comparable to the experimental one for electron energies up to about 60 eV from where on the experimental cross sections are higher irrespective of the impact energy. At $\theta = 30°$ we notice several points: the experimental data display a reversal: at electron energies above 60 eV the 67 keV impact data have a higher cross section, while at electron energies below 20 eV the 48 keV data are higher by a factor of 2. We notice how the CDW calculation for 48 keV falls short at low energies, while being very close at medium electron energies. The present theoretical calculation is quite close to the experimental 48-keV data over a substantial range of energies. As remarked earlier, one could argue that the calculation should be unfolded in energy by 2.5 eV, i.e., the appearance of maxima in these cross sections at electron energies around 5 eV is an artifact of the calculation, which was discussed in the context of Fig. 7.

To test the present theory for the smaller electron energies that are resolved well in the experiment one has to push the calculation to larger internuclear separations. For the sideways emission we found that going from a final separation of 16–31 a.u., reduced a factor-of-four discrepancy at 10 eV to about a factor of 2. A further semiclassical propagation of saddle-point electrons to very large distances has shown that transverse momenta are reduced substantially, and thus one can argue that the extrapolation of the theoretical data to very large distances has the potential to be in accord experiment.

It is possible in the impact-parameter approximation to correlate to some extent the differential electron emission with the closeness of the collision. In Fig. 8 we have shown that forward emission is predominantly produced in $b = 0-2$ a.u. collisions, while intermediate impact parameters play a more substantial role in the sideways emission [note that the curves shown in Fig. 8 are weighted with b when the differential cross section is calculated according to Eq. (8)].

The correlation between impact parameter b and electron energy is provided by Fig. 6. From this graph we concluded that closer collisions produce a significant amount of soft electrons, but at the same time the near-exponential decay of the ionization probability with electron energy is much slower than in distant collisions. The general trend in the doubly differential cross section shown in Fig. 10 is therefore consistent with the somewhat simplistic picture that closer collisions are predominantly responsible for the emission into 0°–50°, while the sideways emission is produced by the intermediate to large impact parameters, and therefore this emission is dominated by soft electrons.

The biggest interest in the present approach is to push it to low ion impact energies where the CDW and CTMC/Born approaches are clearly outside their validity regimes. Both approaches make strong predictions for electron emission to forward angles [12]. It will be important to investigate forward emission experimentally in order to substantiate the claim of cusp formation at large internuclear separations. We

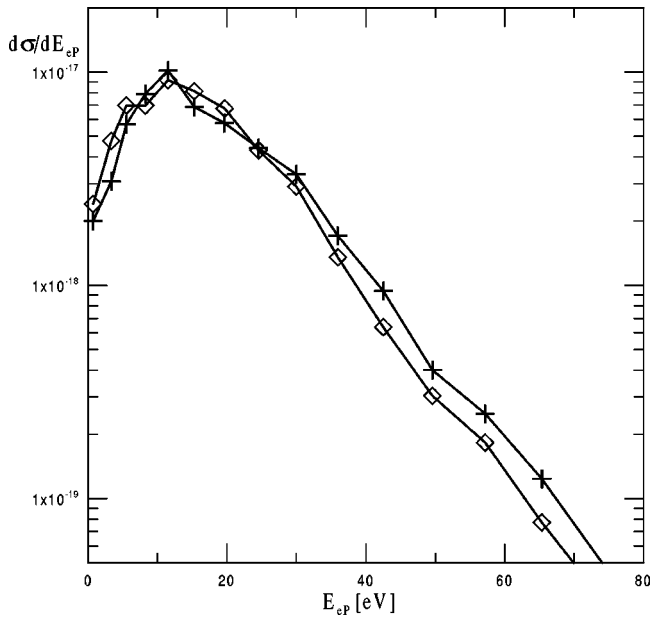

FIG. 11. Singly differential cross section in cm^2/eV for electron emission as a function of energy in the projectile rest frame. Crosses: calculation at final internuclear separation of $R \approx 16$ a.u., diamonds for $R \approx 31$ a.u.

note that these cusps are formed out of electrons that are initially weakly bound by the projectile (otherwise they could not trail the projectile, i.e., be in its vicinity), and which are then field ionized by the target proton. It is not clear at all whether the ($\hbar = 0$) semiclassical approach, i.e., the CTMC method is justified for these electrons. It is possible that substantial differences between quantum and classical calculations will persist in this regime.

An interesting conclusion has been made recently in the CDW approach [27]. A direct relationship was established between the longitudinal recoil momentum distribution and the ionized electron energy spectrum as viewed from the projectile frame. It was argued that the thresholdlike behavior at zero electron energy in this reference frame provided evidence for a cusplike electron energy distribution at the projectile. Given that the prediction of projectile and target cusp electrons is a feature of the CDW approach, and that the numerical solutions of the TDSE show virtually no cusp electrons at the internuclear separations of the order of tens of atomic units, it is of interest to calculate the energy-dependent differential cross section in the projectile frame. Our results given in Fig. 11 for both final internuclear separations indicate that a finite value of the differential cross section at zero energy in the projectile frame is not necessarily associated with cusp electrons. Interestingly the differential cross section rises somewhat in this regime with internuclear separation indicating that the further propagation of the wave packet leads to more ionized electrons at near-zero energy with respect to the projectile. The high-energy tail of the differential cross section is more trustworthy for the calculation at the shorter final separation, as we can see the effect of absorption of fast electrons at the grid boundary in analogy to the discussion given for the target frame in Fig. 5.

IV. CONCLUSIONS

We have carried out three-dimensional solutions to the TDSE for p-H($1s$) collisions in a mixed coordinate/momentum-space approach. Differential ionization probabilities as a function of impact parameter were extracted using a histogram approach based on the momentum mesh, i.e., using a free-particle basis. After integration over impact parameter the singly and doubly differential cross sections were compared with experiment. At electron energies above 20 eV reasonable agreement was found with experiment. At lower energies our analysis technique suffers from the fact that the probabilities were extracted at finite internuclear separations; at a separation of 31 a.u. up to 3 eV average residual binding energy was found for the ionized wave packet. Thus, one has to be careful when analyzing wave packets without an explicit Coulomb wave analysis. Nevertheless, we conclude that our calculated doubly differential cross sections (at $E_P = 56$ keV) generally agree with the experimental data at 48 and 67 keV.

There is a strong need for a reevaluation of the precision of the recommended experimental total ionization cross section in the neighborhood of its maximum. It is remarkable that the CDW calculations agree with the measurements of Shah and Gilbody [22], while theories that incorporate a strong $v_P/2$ mechanism have systematically higher ionization yields, and a somewhat different location for the maximum in the ionization cross section. A possible explanation for the discrepancy between explicit solutions of the TDSE and the CDW method lies in the time histories demonstrated in the present calculations: the CDW method describes the collision as a direct transition from initial to final electron wave functions with some Coulomb correlations between the collision partners. The solutions to the TDSE for impact velocities well above matching suggest that most of the ionized electrons originate at momenta near $v_P/2$, and are then brought closer to the target velocity as a result of the closer geometric proximity of the ionized wave packet to the target nucleus. It is possible that the current CDW method is not able to incorporate this postcollision interaction effect. Given that the proton/antiproton on H($1s$) configurations represent such basic ion-atom collision systems we hope that definitive answers to these questions be found in the immediate future. More detailed comparisons of the present work with experiment and theory at different collision energies will be reported soon.

ACKNOWLEDGMENTS

The financial support by the Natural Sciences and Engineering Council of Canada is gratefully acknowledged. M.H. also thanks Tom Kirchner and Hans-Jürgen Lüdde for many discussions.

[1] T. G. Winter, Phys. Rev. A **37**, 4656 (1988).
[2] N. Toshima, Phys. Rev. A **59**, 1981 (1999).
[3] A. M. Ermolaev, Phys. Lett. A **149**, 151 (1990).
[4] T. G. Winter and C. D. Lin, Phys. Rev. A **29**, 3071 (1984).
[5] O. J. Kroneisen, H. J. Lüdde, T. Kirchner, and R. M. Dreizler, J. Phys. A **32**, 2141 (1999).
[6] T. Kirchner, M. Horbatsch, and H. J. Lüdde, Phys. Rev. A **64**, 012711 (2001).
[7] T. Kirchner and M. Horbatsch, Phys. Rev. A **63**, 062718 (2001).
[8] A. Igarashi, S. Nakazaki, and A. Ohsaki, Phys. Rev. A **61**, 062712 (2000).
[9] J. Fu, M. J. Fitzpatrick, J. F. Reading, and R. Gayet, J. Phys. B **34**, 15 (2001).
[10] M. Horbatsch, in *Application of Accelerators in Research and Industry*, AIP Conf. Proc. No. 392 (AIP, New York, 1997), p. 71; J. Phys. Stud. **1**, 383 (1997).
[11] R. Dörner, H. Khemliche, M. H. Prior, C. L. Cocke, J. A. Gary, R. E. Olson, V. Mergel, J. Ullrich, and H. Schmidt-Böcking, Phys. Rev. Lett. **77**, 4520 (1996).
[12] G. W. Kerby III, M. W. Gealy, Y.-Y. Hsu, M. E. Rudd, D. R. Schultz, and C. O. Reinhold, Phys. Rev. A **51**, 2256 (1995).
[13] L. C. Tribedi, P. Richard, Y. D. Wang, C. D. Lin, and R. E. Olson, Phys. Rev. Lett. **77**, 3767 (1996).
[14] A. Kolakowska, M. S. Pindzola, F. Robicheaux, D. R. Schultz, and J. C. Wells, Phys. Rev. A **58**, 2872 (1998), A. Kolakowska *et al.*, *ibid.* **59**, 3588 (1999); D. R. Schultz *et al.*, Phys. Rev. Lett. **82**, 3976 (1999).
[15] B. M. McLaughlin, T. G. Winter, and J. F. McCann, J. Phys. B **30**, 1043 (1997).
[16] M. Chassid and M. Horbatsch, J. Phys. B **31**, 515 (1998).
[17] E. Y. Sidky and C. D. Lin, J. Phys. B **31**, 2949 (1998); Phys. Rev. A **60**, 377 (1999).
[18] B. Pons, Phys. Rev. A **63**, 012704 (2001); **64**, 019904 (2001); C. Illescas, B. Pons, and A. Riera, *ibid.* **63**, 062722 (2001).
[19] E. Y. Sidky, C. Illescas, and C. D. Lin, Phys. Rev. Lett. **85**, 1634 (2000); J. Phys. B **34**, L163 (2001).
[20] F. D. Colavecchia, G. Gasaneo, and C. R. Garibotti, J. Phys. B **33**, L467 (2000); P. A. Macri *et al.*, Phys. Rev. A **57**, 2223 (1998).
[21] S. Sahoo, K. Roy, N. C. Sil, and S. C. Mukherjee, Phys. Rev. A **59**, 275 (1999).
[22] M. B. Shah and H. B. Gilbody, J. Phys. B **14**, 2361 (1981); M. B. Shah, D. S. Elliot, and H. B. Gilbody, *ibid.* **20**, 2481 (1987).
[23] M. D. Feit, J. A. Fleck, Jr., and A. Steiger, J. Comput. Phys. **47**, 412 (1982).
[24] P. L. Grande and G. Schiwietz, Phys. Rev. A **44**, 2984 (1991).
[25] S. Yu. Ovchinnikov and J. H. Macek, Phys. Rev. Lett. **75**, 2474 (1995).
[26] D. S. F. Crothers and J. F. McCann, J. Phys. B **16**, 3229 (1983); P. D. Fainstein, V. H. Ponce, and R. D. Rivarola, J. Phys. B **24**, 3091 (1991).
[27] V. D. Rodriguez, Y. D. Wang, and C. D. Lin, Phys. Rev. A **52**, 9R (1995); Th. Weber *et al.*, Phys. Rev. Lett. **86**, 224 (2001).